NeuroImage 193 (2019) 57–66

Contents lists available at ScienceDirect

NeuroImage

journal homepage: www.elsevier.com/locate/neuroimage

# Neuronal signatures of a random-dot motion comparison task

Alexander von Lautz [a,b,*], Jan Herding [a,b], Felix Blankenburg [a,b]

[a] Neurocomputation and Neuroimaging Unit, Department of Education and Psychology, Freie Universität Berlin, Habelschwerdter Allee 45, 14195, Berlin, Germany
[b] Bernstein Center for Computational Neuroscience Berlin, Philippstr. 13, 10115, Berlin, Germany

ARTICLE INFO

*Keywords:*
Random-dot motion
Working memory
Decision making
EEG
Centro-parietal positivity
Beta oscillations
Sequential comparison

ABSTRACT

The study of perceptual decision making has made significant progress owing to major contributions from two experimental paradigms: the sequential vibrotactile frequency comparison task for the somatosensory domain requiring working memory, and the random-dot motion task in the visual domain requiring evidence accumulation over time. On the one hand, electrophysiological recordings in nonhuman primates and humans have identified changes in firing rates and power modulations of beta band oscillations with the vibrotactile frequencies held in working memory, as well as with the mental operation required for decision making. On the other hand, firing rates and centro-parietal potentials were found to increase to a fixed level at the time of responding during the random-dot motion task, possibly reflecting an underlying evidence accumulation mechanism until a decision threshold is met. Here, to bridge these two paradigms, we presented two visual random-dot motion stimuli in a sequential comparison task while recording EEG from human volunteers. We identified a modulation of prefrontal beta band power that scaled with the level of dot motion coherence of the first stimulus during a short retention interval. Furthermore, beta power in premotor areas was modulated by participants' choices approximately 700 ms before responses were given via button press. At the same time, dot motion patches of the second stimulus evoked a pattern of broadband centro-parietal signal build-up till responses were made, whose peak varied with trial difficulty. Hence, we show that known modulations of beta power during working memory and decision making extend from the vibrotactile to the visual domain and provide support for the notion of evidence accumulation as an unconfined decision-making mechanism generalizing over distinct decision types.

## 1. Introduction

The study of perceptual decision making investigates how the brain translates sensory information to inform decisions (Heekeren et al., 2008; Shadlen and Kiani, 2013). Investigations into the neural basis of this process have made significant progress with the use of two tasks: (1) the sequential vibrotactile frequency comparison (SFC) task and (2) the visual random-dot motion (RDM) task (for review, see: Gold and Shadlen, 2007).

In vibrotactile SFC experiments participants are tasked with the differentiation of two sequentially presented somatosensory stimuli, vibrating at frequencies f1 and f2, who are set apart by a short working memory (WM) delay. After both vibrotactile frequencies are presented, decisions about whether f2 was higher or lower than f1 are reported by button press. Single-cell recordings in monkeys demonstrate that while retaining f1 in working memory, neural activity in the PFC is parametrically modulated by the to-be-maintained frequency, both in firing rate (Romo et al., 1999) and small neuronal populations' states (Barak et al., 2010). Moreover, following perception of f2, firing rates in the medial and ventral premotor cortex (m/vPMC) reflect the mental calculation f2-f1 necessary to perform the task (Romo et al., 2004; Hernández et al., 2002). Analogous human M/EEG recordings have found corresponding parametric modulations in prefrontal beta band power with the frequency held in working memory (Spitzer et al., 2010; Spitzer and Blankenburg, 2011; von Lautz et al., 2017; Ludwig et al., 2018) and recently a choice-selective beta power change during the formation of a decision in this paradigm (Herding et al., 2016, 2017; Ludwig et al., 2018).

The second task, the discrimination of random-dot motion, requires participants to detect the overall motion direction of a field of moving dots by accumulating across the entire field and report the perceived motion direction via oculomotor responses. This decision process is driven by orientation selective neurons in the middle temporal area (MT) which project to response related areas, such as the lateral intraparietal

* Corresponding author. Neurocomputation and Neuroimaging Unit, Department of Education and Psychology, Freie Universität Berlin, Habelschwerdter Allee 45, 14195, Berlin, Germany.
*E-mail address:* alexander.von-lautz@bccn-berlin.de (A. von Lautz).

https://doi.org/10.1016/j.neuroimage.2019.02.071
Received 12 September 2018; Received in revised form 21 January 2019; Accepted 28 February 2019
Available online 5 March 2019

area (LIP), frontal eye fields (FEF), superior colliculus (SC) and dorsolateral prefrontal cortex (dlPFC) (Ditterich et al., 2003; Kim and Shadlen, 1999; Ratcliff et al., 2003; Shadlen et al., 1996, 2001). Examining broadband signals of the human EEG during a variety of similar paradigms revealed a centro-parietal positivity (CPP; in fact, the classic P300; see Twomey et al., 2015) that built-up until the time of responding and exerted a pattern reflecting the rate of evidence accumulation during single trials (O'Connell et al., 2012; Kelly and O'Connell, 2013; Philiastides et al., 2014).

Curiously, until now human neuroimaging studies have neither investigated the SFC task with RDM stimuli nor the RDM task with vibrotactile stimuli (but see pupil dilation: Urai et al., 2017; monkey LFP: Wimmer et al., 2016). This is particularly surprising, because there is evidence that the SFC task can be applied to other sensory domains (Spitzer and Blankenburg, 2012) and motion direction can be perceived from tactile inputs (van Kemenade et al., 2014; Krebber et al., 2015). Here, we take a first step to reconcile these two avenues of research experimentally by using the classic visual random-dot motion stimuli in a sequential comparison task. While measuring EEG, we consecutively presented two random-dot stimuli and gave participants the task of comparing the magnitude of coherent motion. We hypothesize that the magnitude of motion coherence held in WM is reflected by a parametric modulation of prefrontal beta power and that beta oscillations encode the choice (S2>S1, S2<S1) prior to responding. Moreover, we expect the RDM stimuli to elicit typical responses from occipital channels during stimulus perception and a modulation of the CPP build-up by the amount of available decision evidence. Notably, the decision evidence in the current paradigm is not solely determined by the coherence level of a single RDM stimulus, but by the difference in coherent motion between two RDM stimuli.

## 2. Materials and methods

### 2.1. Participants

Twenty-nine healthy volunteers (20–34 years; 14 female) participated in the study after providing written informed consent. Participants received recompense of 10€ per hour. One participant was excluded from the analysis because of EEG equipment failure during recording. The local ethics committee at the Freie Universität Berlin approved the study.

### 2.2. Procedure

Volunteers were asked to observe two consecutively presented random-dot motion stimuli and to indicate whether the second stimulus (S2) displayed more or less coherent motion than the first stimulus (S1) (Fig. 1). Importantly, participants were asked to compare only the amount of coherent motion, while the motion direction was not relevant for the task and could be upwards or downwards. A trial began by a fixation period of 1 s, which was followed by the first RDM stimulus for 0.5 s. After a 1 s delay, a second RDM stimulus appeared for another 0.5 s. Participants then judged whether S2 displayed more coherently moving dots as compared to S1 by pressing a button with their right hand. One half of the participants indicated S2>S1 and S2<S1 by a button press with their middle and index finger, respectively, while the other half responded vice versa. After indicating their choice, participants were informed whether the decision was correct by a color change of the fixation cross (green or red) for 0.3 s. The next trial started after a variable period of 1–1.5 s. Participants were asked to keep their eyes fixated on the central cross throughout the experiment.

After practicing for 64 trials during the EEG setup, participants performed 1024 trials divided into eight blocks with short breaks in between blocks. Participants were instructed to respond as quickly as possible without making errors. Response times (RTs) were defined as the duration between S2 onset and the button press. If a response took longer than 1.5 s, the fixation cross would flicker to remind participants to respond quickly. These slow trials and very fast responses during S2 presentation (<100 ms after S2 offset) were excluded from subsequent data analyses. The overall recording time was about 70 min.

### 2.3. Stimuli

The stimuli were generated using MATLAB R2014a (The MathWorks), employing the variable coherence random dot motion (VCRDM) library for the Psychtoolbox (Brainard, 1997). In a dimly lit room, the stimuli were presented on a TFT monitor (refresh rate: 60 Hz) that was placed 65 cm away from the upright sitting participant.

Random dot stimuli were displayed within a circular aperture with a diameter of 5° visual angle (dva). The placement of dots in each RDM patch followed the standard VCRDM procedure, which utilizes three independent sets of dots. These are presented for one frame at a time and are displaced every three frames. For example, dot group one moves on frames 1, 4, 7 …, while group two is modulated only on frames 2, 5, 8 … etc. These three sets are crucial, because while they create a percept of continuous movement, it is not possible to track a single dot on screen. In the standard dot motion detection task, each dot has a small likelihood of moving coherently, however, the majority is redrawn at a random location. Here, we used a different implementation in which one part of the dots moves in a certain direction, while the others move randomly (as in Hebart et al., 2012). In the present design, the number of dots moving either upwards or downwards was modulated. Hence, if the coherence level was e.g. “45% up”, for every 100 dots, 45 dots consistently moved

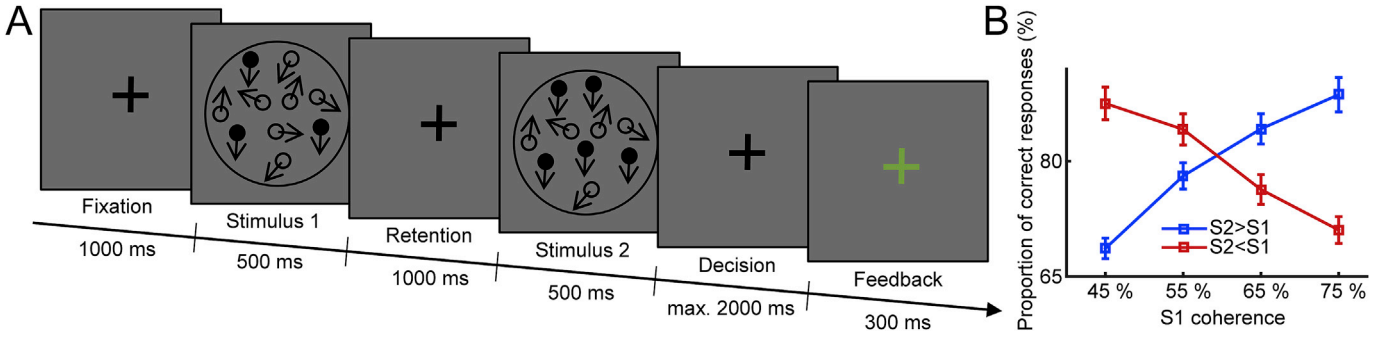


**Fig. 1.** (A) Trial design. A trial started with a 1000 ms fixation period, after which two random-dot motion patches were presented in succession with a delay period of 1000 ms. Each stimulus was on screen for 500 ms and consisted of randomly moving dots, out of which a portion moved non-randomly in the same direction. Participants indicated which of the two patches had more coherent motion while the direction was irrelevant for the task. After responding, participants got feedback by a red or green fixation cross. (B) Overall proportion of correct responses per S1 coherence level for the two possible choices (blue or red). If the coherence level of the second stimulus was higher (choice S2>S1, blue), participants performed better for high coherence S1 trials. If the second stimulus was lower (choice S2<S1, red), higher S1 coherence reduced performance. This is a manifestation of the time-order effect, also termed contraction bias.

upwards, while the remaining 55 moved in random directions. When a dot moved outside the aperture, it was replaced on the opposite boundary with the same inherent motion. The number of dots was fixed at ~2.5 dots/dva$^2$ on screen at a time. Individual dots had a size of ~0.05 dva$^2$ and the motion speed was fixed at 3 deg/s. All these parameters were thoroughly tested to minimize the percept of fuzziness inherent to random dot motion displays.

On each trial, the coherence level for the first stimulus (S1) was randomly set to 45%, 55%, 65%, or 75%, and the coherence level of the second stimulus (S2) varied by ±10 or ±20%. The direction of coherent motion was either up- or downwards and was independent between both RDM patches. Both the proportion of coherent motion and the motion direction were fully counterbalanced throughout the experiment.

### 2.4. Behavioral model

In sequential comparison tasks, the discriminability of stimuli is heavily influenced by the order in which the two stimuli are presented. This effect is known as the time-order error/effect (TOE; e.g., Fechner, 1860; Woodrow, 1935; Hellström, 1985, 2003) or contraction bias (e.g., Ashourian and Loewenstein, 2011). In particular, for a given set of stimuli, participants seem to compare the second stimulus not only with the physical properties of the first stimulus, but also with the average percept from the given stimulus set (Ashourian and Loewenstein, 2011; Karim et al., 2012). In Bayesian terms, participants seem to form a prior which is centered on the mean of the stimulus set and compare the second stimulus with a representation of the first stimulus that was computed by Bayesian inference (i.e., the posterior of the first stimulus). As a consequence, the representation of the first stimulus is shifted towards the overall mean of the stimulus set and can account for the observed behavior associated with the TOE. Here, we used such a Bayesian inference model with a Gaussian prior centered on the set of all coherence levels. The prior variance, stimulus likelihood variance and decision criterion were estimated from the choices of individual participants using variational Bayes with the VBA toolbox (Daunizeau et al., 2014). To quantify the subjectively perceived coherence difference (SPCD) for every trial and each participant, we defined the expected value of the posterior distribution as the mean-shifted percept of S1 (denoted as S1′) to compute S2-S1' (for a more detailed description see Herding et al., 2016 and Sanchez, 2014). The computation of SPCD yielded 16 individual values for each participant that were summarized in six bins representing easy, medium and hard trials (for either choice) to allow for a comparison across the group.

### 2.5. EEG recording and data processing

Sixty-four active electrodes were placed in the extended 10–20 system to record EEG (ActiveTwo, BioSemi) at 2048 Hz. In addition, four electrodes measured the vertical and horizontal electrooculogram (vEOG, hEOG). Each cap was centered on the head and every participants' electrode placement was measured in 3D with a stereotactic electrode-positioning system (Zebris Medical GmbH, Isny, Germany). Each recording was downsampled to 512 Hz, re-referenced to a common average montage and then bandpass filtered between 0.1 and 96 Hz. Line noise at 50 Hz was removed by an additional linear filter using the discrete Fourier transform. The vEOG recording was used to calibrate an adaptive spatial filter that reflected individual eye blinks. These templates were used to inform the removal of eye-blinks (Ille et al., 2002). The blink-free data was cut into epochs of −3 to +3 s relative to S2 onset to investigate stimulus processing and working memory effects. To examine decision-related activity, we alternatively epoched the data with respect to the time of response on each trial. A final visual inspection of each individual trial ensured the removal of artefactual and noisy trials (~16% of trials removed).

For time-frequency (TF) analysis, the Fourier transform of the epoched data was computed separately for low (5–48Hz) and high (40–80Hz) parts of the frequency spectrum. For low frequencies we used an adaptive sliding window of 5 cycles per frequency at 2 Hz steps and multiplied a Hann taper to the data prior to Fourier transformation (i.e., TF bin = 2 Hz × 25 ms). For higher frequencies, we used a multitaper approach based on Slepian sequences with a fixed length of 200 ms at steps of 4 Hz (i.e., TF bin = 4 Hz × 25 ms) and the application of 3 tapers resulting in 10Hz frequency smoothing. Evoked power was calculated by averaging over trials before TF-transformation, while induced averaging was done after the transformation. In addition, to only keep the induced response, we subtracted the evoked response from each trial.

All data analysis was performed using FieldTrip (Radboud University Nijmegen, Donders Institute; fieltriptoolbox.org) and SPM12 (Wellcome Department of Cognitive Neurology, London, UK; www.fil.ion.ucl.ac.uk/spm).

### 2.6. Statistical analysis

The response-locked and S2-locked data were analyzed in analogy. In case of TF transformed data, response-locked TF maps were square root transformed and smoothed with a 3 Hz × 300 ms full width at half maximum Gaussian kernel, reducing between-subject variance (Kilner et al., 2005). To identify the difference between decisions (S2>S1 vs. S2<S1) we performed a general linear model (GLM) analysis with the factors "S2 more/less than S1" and "correct/incorrect" (2x2). Then, we contrasted the individual subject's averages to map the difference between choices. These individual time courses or TF maps then underwent a cluster-based permutation test procedure (Maris and Oostenveld, 2007). The resulting test statistic identifies clusters of strong activity differences and corrects for the family-wise error (FWE) level over channel, time and when applicable also frequency (p_cluster<0.05). The reported test statistic of the TF maps always reflects a cluster correction over relevant time, frequency and channels, specifically the whole WM-interval and the whole time when decisions were made (from S2 onset to button press) and was thresholded at this FWE-corrected alpha at 0.05. The analysis of S2-locked data followed the same procedure but included a baseline correction to the prestimulus fixation period (−0.65 to −0.15 s relative to S1 onset) instead of a square root transformation, because we used this data primarily to investigate WM effects. The GLM factor in addition to correctness was in this case the parametric modulation of S1 coherence level at four levels [45% 55% 65% 75%], which was then zero-mean contrasted [-1.5 -0.5 0.5 1.5]. Hence, the S2-locked contrast shows the parametric modulation of neural activity by the coherence level of S1.

### 2.7. Source reconstruction

The scalp-level effects identified in the previous step were localized in the cortex using the individually recorded electrode positions for each participant and routines applying 3D source reconstruction with multiple sparse priors (MSP) provided by SPM12 (Friston et al., 2006). First, we constructed a forward model using an 8196-point cortical mesh of dipoles distributed perpendicular to a template brain's cortical surface. A three-shell Boundary Elements Method (BEM) EEG head model was used to compute the lead field. Source inversion of the forward model was computed using MSP (Friston et al., 2008) under group constraints (Litvak and Friston, 2008). This was done for each condition for the significant time-frequency window from sensor-level analysis. The source inverted 3D images of each condition were then contrasted in analogy to sensor space analysis and subsequently used for statistical analysis on the group level (cf. Litvak et al., 2011a,b). Mass-univariate statistical testing resulted in significance tests for all voxels. For illustration purposes, we display the significant voxels of each analysis at $p < 0.05$ (uncorrected), indicating the most likely sources of the FWE-corrected sensor level analysis. The above-threshold sources were attributed to anatomical landmarks by employing SPM anatomy toolbox (Eickhoff et al., 2005).

### 2.8. Data and code availability statement

All data and code are available upon request by message to the corresponding author. Use and sharing of this data must comply with the General Data Protection (GDPR) of the European Union and with ethics approval of the Free University Berlin.

## 3. Results

### 3.1. Behavior

Overall, participants responded correctly in 78.5 (7.1) % of trials and with an average RT of 838 (29) ms across conditions (Table 1). A repeated-measures ANOVA of median RTs with the factors "difficulty" (±20% versus ±10% dot-motion coherence) and "sign" (S1>S2 versus S1<S2) identified behavioral differences arising from the tasks' difficulty and the direction of choice. We performed the same analysis on the logit-transformed proportion of correct responses, which was only modulated by the difficulty of the coherence comparison and not the sign. Thus, participants were overall faster when choosing S2<S1, independent of whether their choice was correct. To establish that this difference was not explained by the counterbalanced finger assignment across participants for either S1>S2 or S1<S2, we calculated between groups t-tests for reaction time and performance, which were not significant (RT: $T(13) = 1.37$, $p = 0.19$; PCR: $T(13) = 0.14$, $p = 0.89$). To exclude the possibility that different motion directions influenced behaviour, we compared performance between up- and downward motion (RT: $T(27) = 1.29$, $p = 0.21$; PCR: $T(27) = 0.98$, $p = 0.34$).

Furthermore, we tested whether volunteers performed better in those trials in which the direction of both S1 and S2 was the same, compared to those where dot-motion was different (RT: $T(27) = 0.13$, $p = 0.90$; PCR: $T(2.79)$, $p = 0.009$). Hence, when there were no differences between stimulus directions, participants responded more often correct, but equally fast, as compared with when both RDM stimuli had the same inherent motion.

Interestingly, we observed a pronounced time-order effect/error (contraction bias) that is characteristic for sequential comparison tasks (see Fig. 1B; Herding et al., 2016, 2017; Karim et al., 2012; Ashourian and Loewenstein, 2011; Preuschhof et al., 2010; Woodrow, 1935; Fechner, 1860). In particular, we observed an increase in correct S1<S2 choices with higher S1 stimulus coherence, concurrent with an increase in correct S1>S2 choices with decreasing S1 coherence. This pattern indicates that participants might compare S2 with a representation of S1 that regressed to the mean of the stimulus set (S1′). To account for this substantial effect on performance, we used a behavioral model that estimates the subjectively perceived coherence difference (S2-S1'; SPCD) for each participant and all choices (see Methods: Behavioral model).

### 3.2. Overall stimulus responses

As a first EEG analysis step, we verified that our novel task design showed well-documented patterns in response to random-dot motion stimuli presentation. Fig. 2A illustrates the TF representation of overall changes in stimulus-evoked power relative to a prestimulus baseline.

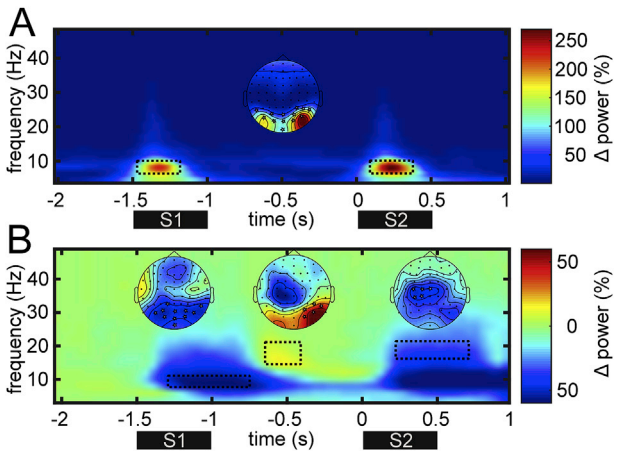


**Fig. 2.** Stimulus-evoked and stimulus-induced time-frequency maps. (A) Grand average of relative change in stimulus-evoked power at 5–48Hz with respect to prestimulus baseline. Data is collapsed over all channels; the topography corresponds to the TF windows during stimulus presentation marked below. (B) Grand average of stimulus-induced power, expressed as the change in power to a prestimulus baseline. The topographies reflect the time-frequency window marked in the boxes below.

Most notably, evoked alpha (7–13 Hz) power increased after stimulus onset, most pronounced in right occipital channels. In addition to overall evoked response, we investigated the overall induced power, as depicted in Fig. 2B. We found a well-established pattern of induced alpha power decreases after stimulus onset relative to the prestimulus baseline (e.g., de Lange et al., 2013; all $p_{\_FWE}<0.05$). Starting about 0.1 s after each stimulus onset, occipital channels showed this alpha decrease while dot-motion was onscreen, with a dimming of the effect after (e.g. 0.5–1 s after S1). While induced alpha power was decreased throughout the task, induced power in the lower beta band at 16–22 Hz first decreased during stimulus presentation but rebounded in right occipital channels after the RDM pattern disappeared (0.3–0.6 s after S1). Then, during the perception of S2 and the start of decision processes, we observed a decrease in induced beta power over contralateral (left) premotor cortex, mimicking effects previously observed in the somatosensory SFC tasks (Herding et al., 2016) that fit with choice-related beta modulations associated with button presses when responding with either hand (Donner et al., 2009; de Lange et al., 2013). This was particularly interesting, because beta band oscillations at 15–25 Hz are typically associated with sensorimotor processing (e.g., Bauer et al., 2006; Van Ede et al., 2011; Pfurtscheller, 1981) and while we did not observe the same pattern as tactile comparison tasks elicit, our subsequent working memory and decision making effects mirrored somatosensory modulations in the beta band (Spitzer et al., 2010; Spitzer and Blankenburg, 2011, 2012; Herding et al., 2016, 2017; Ludwig et al., 2018; von Lautz et al., 2017), indicating a role for this frequency band beyond somatosensory processes. Because a relationship of alpha responses with behavior had been previously reported in a similar task (Haegens et al., 2010), we correlated both the alpha and beta band responses with participants' overall task performance but found no such effect (both $r(27)<0.1$, $p > 0.05$).

**Table 1**
Proportion of correct responses and reaction times for the physical coherence difference S2-S1. Mean values with SD are shown in the left part, the effects are the result of an ANOVA with difficulty and sign as factors. The analysis of difficulty compares the easy (±20) with hard (±10%) trials, the sign effect the positive (+10% and +20%) with the negative (−10% and −20%) coherence difference. As expected, participants were better and faster on easy trials. Interestingly, while participants performed equally on positive and negative trials, they were faster on negative trials (S2<S1). There was no interaction between difficulty and sign.

| | Coherence level difference (S2-S1) | | | | Difficulty effect | Sign effect | Interaction |
|---|---|---|---|---|---|---|---|
| | −20% | −10% | 10% | 20% | F(1, 27) | F(1, 27) | F(1, 27) |
| PCR (%) | 86.3 (6.6) | 70.7 (6.6) | 71.7 (7.8) | 85.15 (7.3) | 242.4*, p < 0.001 | 0.1, p = 0.907 | 3.8, p = 0.061 |
| RT (ms) | 805 (27) | 837 (27) | 855 (30) | 834 (29) | 8.1* p = 0.008 | 35.1*, p < 0.001 | 3.2, p = 0.083 |

### 3.3. Parametric working memory of S1 stimulus coherence

One of the central findings of previous somatosensory working memory M/EEG studies is the parametric modulation of oscillatory power in the beta band as a function of the vibrotactile frequency held in WM (Spitzer et al., 2010; von Lautz et al., 2017). Here, we focused on an analogous stimulus property – the level of dot-motion coherence. The TF map in Fig. 3 depicts the parametric contrast of the four motion coherence levels (45%, 55%, 65%, 75%) during stimulus retention. The permutation test procedure identified a cluster from right prefrontal channels in the beta band (18–26Hz) that was modulated by the to-be-remembered stimulus coherence 0.4–0.8 s after S1 offset ($p_{\_FWE}<0.05$). Source reconstruction of this cluster with the same parametric constrast placed this effect in the bilateral inferior frontal gyrus (peak MNI: +42,+36,+14; Fig. 3C). Notably, the timecourse of this frontal beta band modulation (Fig. 3D) showed an overall increase in ERS at the center of the working memory interval whose peak was monotonically greater for higher stimulus coherences held in working memory, as indicated by linear trend analysis (0.45–0.7s, all time bins $p < 0.05$).

Exploratory analysis of higher frequencies (>48Hz) revealed a parametric modulation of gamma power at 55–65 Hz throughout the whole WM interval ($p_{\_FWE}<0.05$; Supplementary Fig. 1A). Interestingly, while beta power increased with stimulus frequency, gamma power decreased. The source of this activity was localized to a large portion in the right inferior frontal gyrus (IFG; peak MNI: +52,+24,+0) (Supplementary Fig. 1C). However, the analysis of the gamma band timecourse revealed that the highest coherence condition alone was mainly driving this effect (Supplementary Fig. 1B).

Unexpectedly, we identified a cluster of centro-parietal channels whose lower beta power was modulated by S1 stimulus coherency ($p_{\_FWE}<0.05$, Supplementary Fig. 1D). The timecourse of this effect (Supplementary Fig. 1E) showed the same beta power peak as observed in higher beta frequencies (cf. Fig. 3D), however, displaying a monotonic decrease with higher stimulus coherence (linear trend 0–0.15 s and 0.5–0.65 s, at $p_{\_FWE}<0.05$). Source reconstruction revealed bilateral area 4a of the primary motor cortex as the origin of this negative modulation (peak MNI: +4, −36, +66) and the precuneus (peak MNI: −16, −54,+68; Supplementary Fig. 1F).

### 3.4. Beta band indexes subsequent choice

To investigate the oscillatory signatures underlying decision making we contrasted trials by participants' choices: S2 > S1 vs. S2 < S1. This analysis revealed a central cluster in frequencies of 20–30 Hz at 0.9–0.6 s before answering ($p_{\_FWE}<0.05$). The focal pattern in topography (Fig, 4 C) as well as source reconstruction (Fig. 4, B) pinpointed the location of this effect to bilateral (pre-) motor cortices (Area 4a, peak MNI: −6, −14, 72).

We applied our model of subjectively perceived coherence difference (SPCD) that accounts for the time-order effect on every trial to the analysis of the average central beta band time course. The resulting trials were binned in six groups, from perceiving much more coherency in S2 than S1 to the opposite. Fig. 4D illustrates the beta band modulation by each separate SPCD bin and Fig. 4E separated by choice, indicating a stronger central beta for S2>S1 trials 0.9–0.5 s before responding. If this beta band effect reflects subjects' choice, incorrect trials are expected to show the inverse pattern, because participants chose the opposite answer. Analysis of the average beta band time courses did indeed indicate this opposite pattern (Fig. 4D, bottom right), but was not significantly modulated, likely due to the small amount of incorrect choices.

### 3.5. Centro-parietal positivity

We used the subjectively perceived coherence differences (i.e. S2-S1′) estimated for each trial as regressors for the analysis of stimulus- and response-locked epochs (Fig. 5, *top* and *bottom* respectively). Thus, we contrasted not only trials by participants' choice, but also by how difficult each choice was in turn.

A positive modulation of centro-parietal ERPs after S2 onset was clearly visible over a set of 17 electrodes marked in the scalp topography

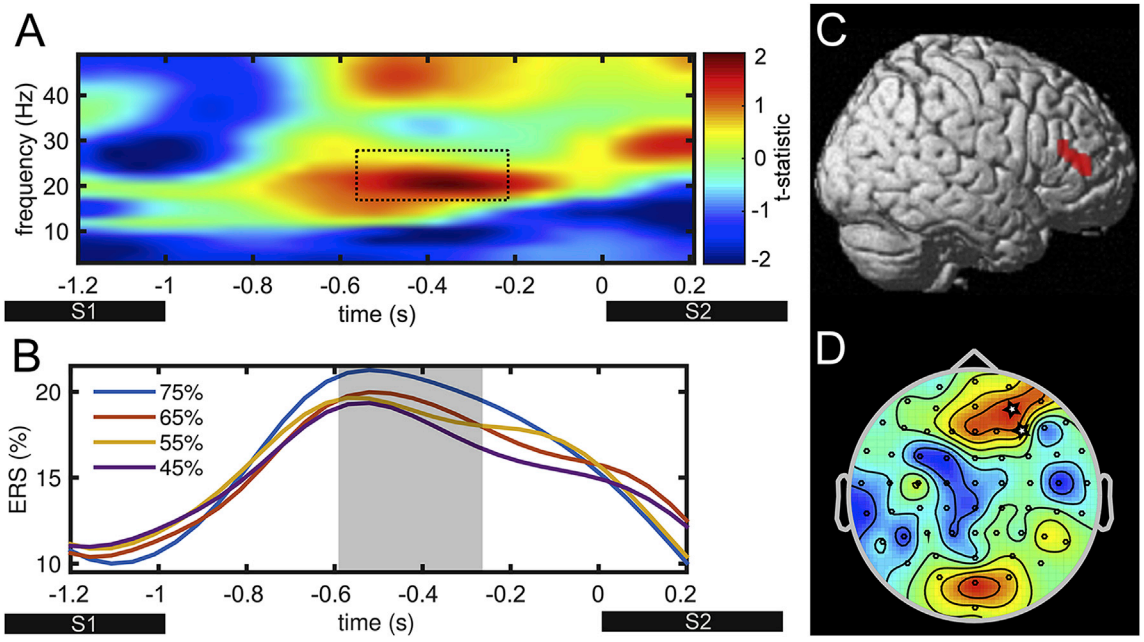


**Fig. 3.** TF analysis and source reconstruction reveal parametric representation in right prefrontal beta band. (A) Time-frequency map of the zero-mean contrast of low to high coherence levels (45–75%) across channels F4 and AF4. (B) Time course of the average beta band per S1 coherence level during the retention interval. The grey mark depicts significant time points of linear trend analysis ($p < 0.05$). (C) Source reconstruction of the beta band effect identified with nonparametric cluster analysis marked in A. The most likely source of this prefrontal effect was found in the right IFG. The red marking shows the thresholded 3D source ($p < 0.05$, uncorrected). (D) Topography of the cluster identified in A, corresponding to the source reconstruction in C.

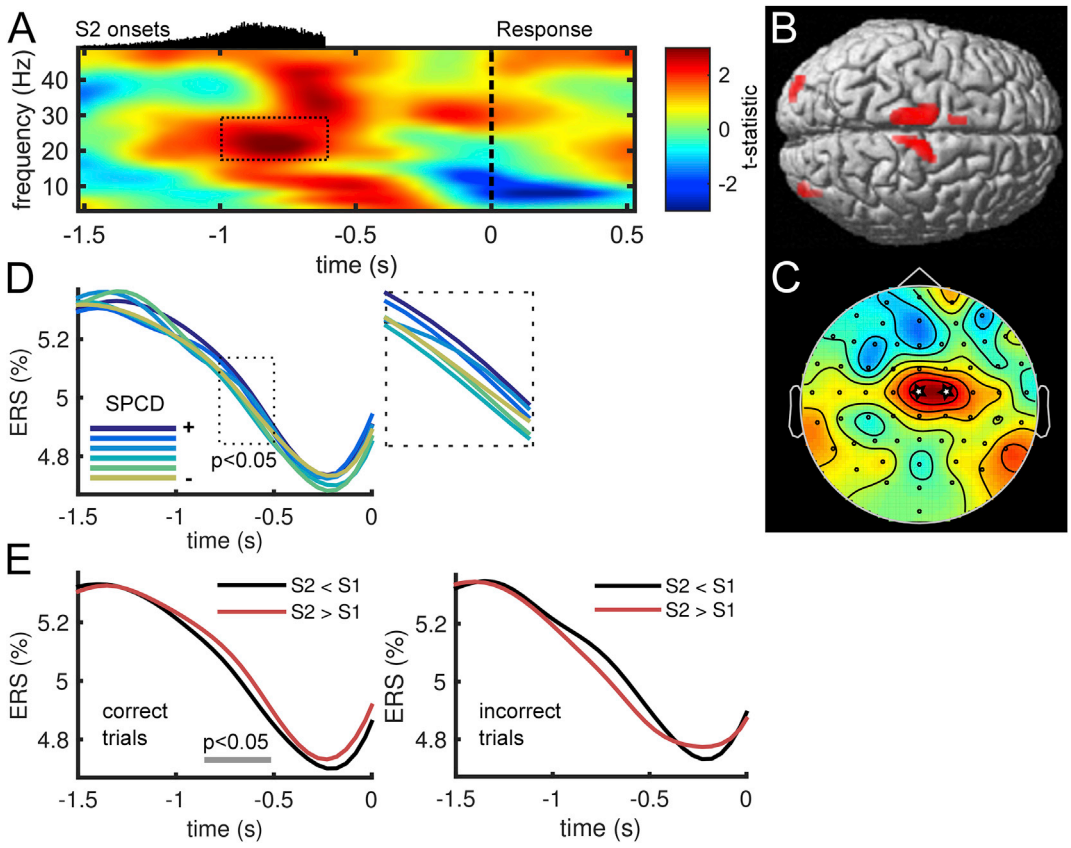


**Fig. 4.** Choice-modulated power in upper beta band. (A) Time-frequency representation of response-locked power in t-values of choice contrast (S2>S1 vs. S2<S1) averaged over electrodes Cz and C2. Histogram above the TF map depicts the distribution of S2 onsets. Nonparametric cluster analysis revealed a modulation of the beta band by choice, marked here with the black box. (B) Result of 3D source reconstruction of the significant cluster marked in the time-frequency window in A. The effect was rendered on a T1 standard brain, red marks the areas of most likely sources, thresholded at $p < 0.05$ uncorrected. (C) Topography of the central cluster marked by the box in A. (D) Time course of beta band power from central channels grouped by the subjectively perceived coherence difference (SPCD) in six levels. Inset zooms into the significant time window, showing a binary split between higher and lower perceived coherence differences. (E) Left: Time course of beta power for correct trials, split by subsequent choice. Gray line marks the time of statistical significance of these time courses ($p < 0.05$). Right: Time course of beta power as on the left but for incorrect trials, split into S2 higher or lower than S1, and showing the opposite pattern (n.s.).

in Fig. 5 ($p_{\_FWE}<0.001$), closely matching the classic P300 and typical CPP topographies. We collapsed analyses across both up- and downward motion as there was no influence on CPP amplitude, latency and topography (all $p > 0.05$). In general, the CPP built up shortly after stimulus onset (0.2s) and flattened out immediately after stimulus offset (0.5 s).

Comparing choices of S2>S1 with S2<S1 revealed a modulation of the CPP between 0.2 and 0.4 s after S2 onset and a later, likely response related difference starting after 0.75s (thresholded at $p_{\_FWE}<0.05$, Fig. 5, *top left*). The observation that responses of S2<S1 were slightly faster (see Table 1), may therefore be explained by faster CPP build-up. Subsequently, we split correct trials into subjectively perceived bins of 'easy', 'medium', and 'hard' trials according to our behavioral model. The top right part of Fig. 5 illustrates that the CPP increased in proportion to the strength of S2-S1′ coherence difference and correspondingly had a higher peak level (0.4–0.92s, $p_{\_FWE}<0.05$). We were interested, whether this pattern extended to incorrect trials, and found a slower build-up and lower peak CPP as early as 0.3s after stimulus onset when compared to the average correct response (threshold at $p_{\_FWE}<0.05$).

Analogous analysis of response-locked data revealed a build-up of centro-parietal signals from 22 channels that was most pronounced over left posterior parietal areas ($p_{\_FWE}<0.001$, Fig. 5 topography, *bottom*). Contrary to S2-locked signals this accumulation of signal peaked with the response button press and dropped to baseline levels shortly after. Subjects' choices modulated this signal, with an increased CPP build-up for S2>S1 trials in the last 200 ms before responding ($p_{\_FWE}<0.05$). Split into bins of 'easy', 'medium' and 'hard' trials, we found a proportional CPP peak at response that scaled with difficulty and was reduced in incorrect trials (both thresholded at $p_{\_FWE}<0.05$).

Previous RDM studies tasking participants with motion detection in only one RDM stimulus, cannot readily separate the perceptual aspects of motion detection from the accumulation of evidence for a decision. In the present task however, we are able to separate the two processes, because S1 is perceived without an immediate decision. Therefore, to underline that the observed CPP effects represent a decision variable and not sensory evidence in the motion perception of RDM stimuli, we investigated the build-up of CPP relative to S2 stimulus coherence, as this could represent an accumulation of sensory evidence for the stimulus coherence level rather than the decision of S2-S1'. We constructed a parametric contrast of the eight levels (25%, 35%, …, 95%) of S2 coherence and tested this against zero with the same permutation test procedure as in previous analyses. This investigation did not indicate any effect of S2 stimulus coherence on the CPP time course (all clusters $p_{\_FWE}>0.05$). Since the S2 coherence is confounded with the difficulty of the task-relevant S2-S1 calculation, we also applied this analysis to the S1 coherence, again with no significant results (all clusters $p_{\_FWE}>0.05$). Fig. 6 depicts the CPP responses to S1 and S2 for each of the different coherence levels. Notably, the overall CPP response was a lot lower in response to S1 when comparing to that of S2. In addition, we observed the strongest CPP responses after those stimuli, which gave the most information to solve the task (S2 = 25% and S2 = 95%) while the lowest responses were observed when the perception of S2 was not informative by itself (S2 = 55% and S2 = 65%). These control analyses on our

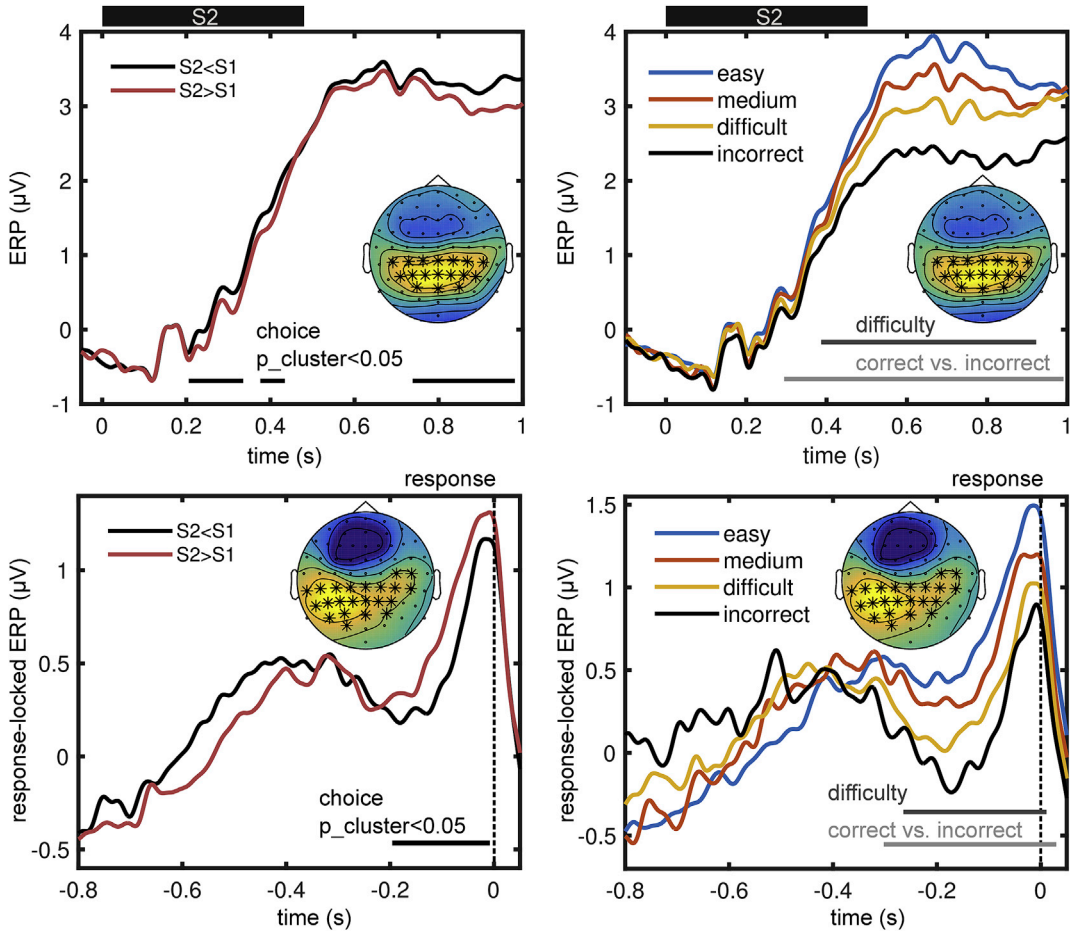


**Fig. 5.** Centro-parietal signal increases with perception of S2 and reaches maximum with response. Top: S2-locked broadband EEG response from channels marked in topography with *. The left part shows time courses of each possible choice, S2>S1 and S2<S1, the right part the modulation by model-based estimates of subjectively perceived coherence difference (SPCD), split into easy, medium, difficult and incorrect trials. Bottom: Same as in figures above, but for response-locked signals and channels from the positive cluster marked in the topography with *. Channels marked in topographies in all plots are those that were significantly modulated for more than 50% of time in significant time window ($p_{\_FWE}<0.05$). Black and grey lines show the significant time windows from the cluster-based permutation analysis for choice (left) and difficulty as well as of correct vs. incorrect trials respectively (right).

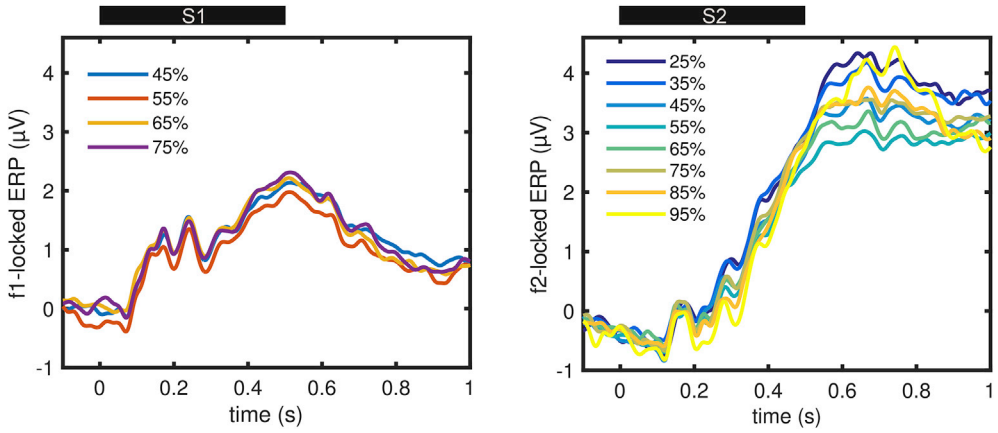


**Fig. 6.** Centro-parietal signal is not systematically modulated by RDM coherency. Left: S1-locked broadband EEG responses from centroparietal channels for each of the four S1 coherence levels. Notably, the CPP is not modulated by the coherence of the response, in contrast with its modulation by difficulty after S2 (see Fig. 5, top right). Moreover, the overall CPP response is lower in response to S1 than it is in response to S2, as seen on the right and also in Fig. 5. Right: S2-locked broadband EEG responses from the same centroparietal channels used in Fig. 5 for each of the eight S2 coherence levels. Note in particular that the highest CPP response is evident in the 25% and 95% condition, where the choice is easiest, and lowest in the 55% and 65%, where the choice is hardest. This is the case, because in e.g. 25% coherence S2 trials, the correct answer is always S2<S1, while in 55% coherence S2 trials both answers are equally likely.

particular task give further evidence that the CPP reflects a true 'decision variable' that tracks decision-relevant evidence and not just sensory input.

## 4. Discussion

We investigated the neural processes underlying working memory and perceptual decisions using a sequential random-dot motion (RDM) coherence comparison task. We identified modulations of the beta band during the retention interval of the task and during the formation of a decision: first, in prefrontal areas, beta band power increased monotonically with the coherence level held in working memory. Second, in premotor and motor areas, participants' choices modulated beta power before responding by button press. Additionally, the CPP tracked the accumulation of decision-relevant evidence, reflecting the subjectively perceived coherence differences between the two RDM patches, indexing the trial difficulty. Our results suggest that inferior frontal (WM), posterior parietal (CPP), and motor regions (choice) work together to maintain and evaluate decision related stimulus features independent of sensory modality.

In remarkable agreement with previous reports of vibrotactile parametric working memory recorded with MEG, EEG, and fMRI in humans (von Lautz et al., 2017; Spitzer et al., 2010; Kostopoulos et al., 2007; Wu et al., 2018) and single-cell recordings in nonhuman primates (e.g., Romo et al., 1999), we observed a monotonic scaling of beta band power in the right IFG with the RDM coherence held in working memory. Moreover, the observed frequency range (18–26 Hz) and the precise location within the IFG matches results from a visual flicker frequency task more closely than similar tactile or auditory recordings (see Spitzer and Blankenburg, 2012; Wu et al., 2018). In particular, a recent fMRI decoding study employing an SFC task across sensory modalities found WM content-specific activity in the right IFG for both visual and tactile working memory (Wu et al., 2018). Interestingly, in an exploratory analysis we observed a concurrent decrease of prefrontal gamma power with the coherence retained in working memory (Supplementary Figs. 1E–H). This pattern of beta and gamma power was also recently observed with MEG (von Lautz et al., 2017) and is a known correlate of WM (Fuentemilla et al., 2010; Haegens et al., 2010). In contrast to MEG however, EEG may be ill-suited for investigations of high gamma frequencies, because the skull acts as a low-pass filter (Nunez, 1981). Moreover, the observed decrease appeared to be mostly driven by the lowest S1 coherence level alone and may therefore not be as reliable as previous MEG recordings. Together, our findings provide further evidence for a modality independent role of prefrontal beta oscillations for parametric working memory that may be a feature of passive maintenance states interrupted by brief gamma bursts as observed recently during monkey recordings (Lundqvist et al., 2016; Sherman et al., 2016; Stokes, 2015).

In sequential comparison tasks, it is assumed that decisions are the result of mentally calculating stimulus 2 – stimulus 1. Choice-related neural activity is expected to reflect the resulting sign (±) of this subtraction. Fitting with this notion, we found a modulation of beta oscillatory power by choice in central regions associated with the response-button press, for which source reconstruction estimated premotor and motor regions as the most likely sources. This supports the idea that neural responses of decision processes are exhibited in those parts of the brain where subsequent responses are put into action (Shadlen et al., 2008). Our findings agree with vibrotactile comparison tasks in both non-human primates and humans (Haegens et al., 2011; Herding et al., 2016; Ludwig et al., 2018), where power in the upper beta band from bilateral pre-motor areas was modulated by subjects' choices before responding. Remarkably, the same pattern appears to be response-modality specific, as Herding and colleagues (2016, 2017) had participants respond by either button press or saccades and found distinct sources of this effect in premotor areas and FEF, respectively. Moreover, firing rate changes reflecting the signed difference between vibrotactile frequencies, f2-f1, have been recorded in medial and ventral PMC when monkeys responded by button press (Hernández et al., 2002, 2010; Romo et al., 2004). Crucially, these studies all used vibrotactile stimuli. In contrast, our present results are the first to demonstrate choice encoding in the beta band from motor areas for a visual sequential comparison task.

Interestingly, recordings during sequential comparisons of visual RDM stimuli have been made in monkey lPFC, where firing rates reflect task-relevant sensory, memory and decision processes (Zaksas and Pasternak, 2006; Hussar & Pasternak, 2012, 2013). Additionally, Wimmer et al. (2016) analyzed LFPs during the same task and found that beta power encoded the task-relevant S1 feature during the working memory delay, matching the present findings (Fig. 3). Moreover, broadband LFP activity reflected the difference between S2 and S1, first in proportion to the stimulus difference (S2-S1), then as an index of choice. While not in the same area, these effects are similar to previous sensorimotor LFP recordings during a vibrotactile version (Haegens et al., 2011) and have been theorized to communicate in a top-down fashion with MT and motor areas in a hierarchical network (Wimmer et al., 2016). Agreeing with this idea, we speculate that the present findings complement previous single-cell recordings by showing the analogous modulatory effects in synchronized neuronal population activity.

Our findings in the beta band also provide further evidence for a generalized, supramodal role for the beta band in encoding task-relevant quantitative information (Spitzer et al., 2014; Spitzer and Blankenburg, 2012; Herding et al., 2016). In this view (for review, see Spitzer and Haegens, 2017), beta band amplitude may reflect quantities at different times of such comparison tasks in distinct brain areas, i.e. lPFC during parametric coherence level retention (Barak et al., 2010; Brody et al., 2003; Romo et al., 1999) and PMC during decision making (Haegens et al., 2011; Herding et al., 2016; Hernández et al., 2002), as a dynamic, short-lived brain state for endogenous information processing. Additionally, in a recent EEG study using an SFC task with delayed decision reports, Ludwig et al. (2018) demonstrated that premotor beta power only indexed choices when a specific motor mapping was provided during the decision delay, thereby further extending this view to necessitate immediate task-relevance of the encoded choice. In the present design, both working memory and decision information were immediately pertinent to the task, as the retention interval was short with one second and the decision was not delayed, but responses given immediately. Therefore, our task is suitable to investigate whether we can extend our understanding of this quantity- and choice-related signal to the visual domain, providing evidence for a common quantitative task-relevant code in the beta band irrespective of sensory modality. Additionally, the decision variable reflected the calculation of S2-S1 and not the accumulation of evidence for any particular motion direction directly, as in the typical RDM paradigm. We therefore speculate that when applying the present task to recordings in nonhuman primates, we may be able to separate the sensory and perceptual aspects of decision making and relate them to the functioning of MT and LIP/VIP neurons (cf. Huk et al., 2017; Katz et al., 2016). Such recordings may also serve to better understand the association of beta amplitude and decision accuracy, as previous MEG recordings where participants responded with either hand have indicated that beta may reflect the accuracy and not the content of upcoming perceptual reports (Donner et al., 2007), for which we found no evidence in the present study where participants responded with one hand only.

Complementing these oscillatory changes, a number of recent studies have suggested that the CPP - a broadband signal in the human EEG - tracks the accumulated evidence for perceptual decisions that require sequentially sampling and integrating input over time (Kelly & O'Connell, 2013; Philiastides et al., 2014; Twomey et al., 2015). In the particular case of RDM tasks, Kelly & O'Connell (2013) observed that the CPP's build-up rate is modulated by the level of coherent motion in the presented RDM patch, irrespective of the motion direction. Overall, the CPP may directly reflect known single-cell firing variability in the PPC with an accumulation of evidence in the form of a decision variable (for

review, see Gold and Shadlen, 2007; Shadlen and Kiani, 2013). The present findings agree with these earlier reports of the CPP and extend the view of the CPP as a token of the current state of decision making. Exceptionally, in our novel task the tracking of the CPP represented not the accumulation of evidence for perceived motion, as known from single-stimulus RDM tasks (see Kelly & O'Connell, 2013), but embodied the imminent decision process, i.e., evidence accumulation for the difference between S1 and S2. Furthermore, we observed a scaling of the CPP with respect to the subjectively perceived coherence difference, and thus the difficulty of the trials. This in turn may indicate that the peak of the CPP (or P300) is related to a participants' confidence in the decision, as previously observed in RDM paradigms with other electrophysiological or neuroimaging methods (Hebart et al., 2016; Kiani and Shadlen, 2009; Ding and Gold, 2012).

Interestingly, we encountered no absolute bound of CPP at the time of the response, as has been observed in recent studies with RDM patches (O'Connell et al., 2012; Kelly & O'Connell, 2013). On the contrary, our investigations agree with findings from face/house decision tasks, where scalp potentials appear to be parametrically scaled by the amount of sensory evidence at the time of choice (Philiastides et al., 2014). Our observations can be explained by a diffusion-to-bound model with collapsing bounds (for an overview, see O'Connell et al., 2018), where the amount of sensory evidence as indexed by the CPP required for a decision decreases over time and is therefore lower for the more difficult, slower trials at the time of response. However, we did not observe a more gradual build-up of CPP for more difficult trials, but rather a small decrease in CPP 200 ms before the participant responded. Therefore, the CPP appears not to index the accumulation of evidence for any single motion direction as in classic RDM paradigms, but the difference in coherence between two of them. Indeed, it may be that the lagged build-up is also a feature of a sensory process in RDM tasks, as this effect was also not observed in a face/house distinction task (cf. Philiastides et al., 2014). To fully understand what the CPP represents, the relation between the CPP in a comparison task and its counterpart with a single RDM stimulus should be investigated directly, and differences and common components (e.g., with cross-classification) investigated.

In conclusion, beta power scaled parametrically with the random dot motion coherence in right prefrontal areas during stimulus retention, then indexed the choice before responding. These effects mirror findings from the well-studied vibrotactile domain with human M/EEG and single-cell recordings in nonhuman primates. Moreover, the CPP accrued before responding and was influenced by the subjectively perceived difficulty on each trial. Notably, the CPP was not affected by RDM motion perception, but changed with the task of comparing two stimuli, indicating a close relationship to the decision variable. The present findings are a first step to unite major lines of decision making paradigms across sensory domains, with findings pointing to an extended role for the beta band during working memory and decision making and to further insights into the CPP as an index of evidence accumulation.

## Conflicts of interest

None.

## Funding

This work was supported by Deutscher Akademischer Austauschdienst; and the German Research Foundation (DFG Grant GRK1589/2).

## Acknowledgements

The authors thank Laurence Hunt, Maria Rüsseler and Timo Schmidt for helpful suggestions as well as Isil Uluc for help during data collection.

## Appendix A. Supplementary data

Supplementary data to this article can be found online at https://doi.org/10.1016/j.neuroimage.2019.02.071.

## References

Ashourian, P., Loewenstein, Y., 2011. Bayesian inference underlies the contraction bias in delayed comparison tasks. PLoS One 6, e19551.
Barak, O., Tsodyks, M., Romo, R., 2010. Neuronal population coding of parametric working memory. J. Neurosci. 30, 9424–9430. https://doi.org/10.1523/JNEUROSCI.1875-10.2010.
Bauer, M., Oostenveld, R., Peeters, M., Fries, P., 2006. Tactile spatial attention enhances gamma-band activity in somatosensory cortex and reduces low-frequency activity in parieto-occipital areas. J. Neurosci. 26, 490–501.
Brainard, D.H., 1997. The psychophysics toolbox. Spat. Vis. 10, 433–436. https://doi.org/10.1163/156856897X00357.
Brody, C.D., Hernández, A., Zainos, A., Romo, R., 2003. Timing and neural encoding of somatosensory parametric working memory in macaque prefrontal cortex. Cereb. Cortex 13, 1196–1207. https://doi.org/10.1093/cercor/bhg100.
Daunizeau, J., Adam, V., Rigoux, L., 2014. VBA: a probabilistic treatment of nonlinear models for neurobiological and behavioural data. PLoS Comput. Biol. 10, e1003441.
de Lange, F.P., Rahnev, D.A., Donner, T.H., Lau, H., 2013. Prestimulus oscillatory activity over motor cortex reflects perceptual expectations. J. Neurosci. 33, 1400–1410. https://doi.org/10.1523/JNEUROSCI.1094-12.2013. PMID 23345216.
Ding, L., Gold, J.I., 2012. Neural correlates of perceptual decision makingbefore, during, and after decision commitment in monkey frontaleyefield. Cereb. Cortex 22, 1052–1067.
Ditterich, J., Mazurek, M.E., Shadlen, M.N., 2003. Microstimulation of visual cortex affects the speed of perceptual decisions. Nat. Neurosci. 6, 891–898.
Donner, T.H., Siegel, M., Oostenveld, R., Fries, P., Bauer, M., Engel, A.K., 2007. Population activity in the human dorsal pathway predicts the accuracy of visual motion detection. J. Neurophysiol. 98, 345–359.
Donner, T.H., Siegel, M., Fries, P., Engel, A.K., 2009. Buildup of choice-predictive activity in human motor cortex during perceptual decisionmaking. Curr. Biol. 19, 1581–1585.
Eickhoff, S.B., Stephan, K.E., Mohlberg, H., Grefkes, C., Fink, G.R., Amunts, K., et al., 2005. A new SPM toolbox for combining probabilistic cytoarchitectonic maps and functional imaging data. Neuroimage 25, 1325–1335. https://doi.org/10.1016/j.neuroimage.2004.12.034.
Fechner, G.T., 1860. Elemente der Psychophysik. Breitkopf & Härtel, Leipzig.
Friston, K., Henson, R., Phillips, C., Mattout, 2006. Bayesian estimation of evoked and induced responses. J. Hum. Brain Mapp. 27 (9), 722–735. Sep;.
Friston, K., Harrison, L., Daunizeau, J., Kiebel, S., Phillips, C., Trujillo-Barreto, N., 2008. Multiple sparse priors for the M/EEG inverse problem. Neuroimage 39, 1104–1120.
Fuentemilla, L., Penny, W.D., Cashdollar, N., Bunzeck, N., Duzel, E., 2010. Theta-coupled periodic replay in working memory. Curr. Biol. 20, 606–612. https://doi.org/10.1016/j.cub.2010.01.057.
Gold, J.I., Shadlen, M.N., 2007. The neural basis of decision making. Annu. Rev. Neurosci. 30, 535574.
Haegens, S., Osipova, D., Oostenveld, R., Jensen, O., 2010. Somatosensory working memory performance in humans depends on both engagement and disengagement of regions in a distributed network. Hum. Brain Mapp. 31, 26–35. https://doi.org/10.1002/hbm.20842.
Haegens, S., Nácher, V., Hernández, A., Luna, R., Jensen, O., Romo, R., 2011. Beta oscillations in the monkey sensorimotor network reflect somatosensory decision making. PNAS 108, 10708–10713.
Hebart, M.N., DonnerTH, Haynes, J.-D., 2012. Human visual and parietal cortex encode visual choices independent of motor plans. Neuroimage 63, 1393–1403.
Hebart, M.N., Schriever, Y., Donner, T.H., Haynes, J.-D., 2016. The relationship between perceptual decision variables and confidence in the human brain. Cereb. Cortex 26, 118–130.
Heekeren, H.R., Marrett, S., Ungerleider, L.G., 2008. The neural systems that mediate human perceptual decision making. Nat. Rev. Neurosci. 9, 467–479. https://doi.org/10.1038/nrn2374.
Hellström, Å., 1985. The time-order error and its relatives: mirrors of cognitive processes in comparing. Psychol. Bull. 97, 35–61.
Hellström, Å., 2003. Comparison is not just subtraction: effects of time- and space-order on subjective stimulus difference. Percept. Psychophys. 65, 1161–1177.
Herding, J., Spitzer, B., Blankenburg, F., 2016. Upper beta band oscillations in human premotor cortex encode subjective choices in a vibrotactile comparison task. J. Cogn. Neurosci. 1–12.
Herding, J., Ludwig, S., Blankenburg, F., 2017. Response-modality-specific encoding of human choices in upper beta-band oscillations during vibrotactile comparisons. Front. Hum. Neurosci. 11.
Hernández, A., Zainos, A., Romo, R., 2002. Temporal evolution of a decision-making process in medial premotor cortex. Neuron 33, 959–972.
Hernández, A., Nácher, V., Luna, R., Zainos, A., Lemus, L., Alvarez, M., 2010. Decoding a perceptual decision process across cortex. Neuron 66, 300–314.
Huk, A.C., Katz, L.N., Yates, J.L., 2017. The Role of the lateral intraparietal area in (the study of) decision making. Annu. Rev. Neurosci. 40, 349–372.
Hussar, C.R., Pasternak, T., 2012. Memory-guided sensory comparisons in the prefrontal cortex: contribution of putative pyramidal cells and interneurons. J. Neurosci. 32 (8), 2747–2761.

Hussar, C.R., Pasternak, T., 2013. Common rules guide comparisons of speed and direction of motion in the dorsolateral prefrontal cortex. J. Neurosci. 33 (3), 972–986.
Ille, N., Berg, P., Scherg, M., 2002. Artifact correction of the ongoing EEG using spatial filters based on artifact and brain signal topographies. J. Clin. Neurophysiol. 19, 113–124. https://doi.org/10.1097/00004691-200203000-00002.
Karim, M., Harris, J.A., Morley, J.W., Breakspear, M., 2012. Prior and present evidence: how prior experience interacts with present information in a perceptual decision making task. PLoS One 7, e37580.
Katz, L., Yates, J., Pillow, J.W., Huk, A., 2016. Dissociated functional significance of choice-related activity across the primate dorsal stream. Nature 535, 285–288. https://doi.org/10.1038/nature18617.
Kelly, S.P., O'Connell, R.G., 2013. Internal and external influences on the rate of sensory evidence accumulation in the human brain. J. Neurosci. 33, 19434–19441. https://doi.org/10.1523/JNEUROSCI.3355-13.2013.
Kiani, R., Shadlen, M.N., 2009. Representation of confidence associated with a decision by neurons in the parietal Cortex. Science 324, 759–764.
Kilner, J.M., Kiebel, S.J., Friston, K.J., 2005. Applications of random field theory to electrophysiology. Neurosci. Lett. 374, 174–178. https://doi.org/10.1016/j.neulet.2004.10.052.
Kim, J.N., Shadlen, M.N., 1999. Neural correlates of a decision in the dorsolateral prefrontal cortex of the macaque. Nat. Neurosci. 2, 176–185. https://doi.org/10.1038/5739.
Kostopoulos, P., Albanese, M.C., Petrides, M., 2007. Ventrolateral prefrontal cortex and tactile memory disambiguation in the human brain. Proc. Natl. Acad. Sci. U.S.A. 104, 10223–10228. https://doi.org/10.1073/pnas.0700253104.
Krebber, M., Harwood, J., Spitzer, B., Keil, J., Senkowski, D., 2015. Visuotactile motion congruence enhances gamma-band activity in visual and somatosensory cortices. Neuroimage 117, 160–169.
Litvak, V., Friston, K., 2008. Electromagnetic source reconstruction for group studies. Neuroimage 42, 1490–1498.
Litvak, V., Mattout, J., Kiebel, S., Phillips, C., Henson, R., Kilner, J., 2011a. EEG and MEG data analysis in SPM8. Comput. Intell. Neurosci. 852961, 2011.
Litvak, V., Mattout, J., Kiebel, S., Phillips, C., Henson, R., Kilner, J., 2011b. EEG and MEG data analysis in SPM8. Comput. Intell. Neurosci. 2011, 852961.
Ludwig, S., Herding, J., Blankenburg, F., 2018. Oscillatory EEG signatures of postponed somatosensory decisions. Hum. Brain Mapp. 1–14. https://doi.org/10.1002/hbm.24198.
Lundqvist, M., Rose, J., Herman, P., Brincat, S.L., Buschman, T.J., Miller, E.K., 2016. Gamma and beta bursts underlie working memory. Neuron 90, 152–164. https://doi.org/10.1016/j.neuron.2016.02.028.
Maris, E., Oostenveld, R., 2007. Nonparametric statistical testing of EEG- and MEG-data. J. Neurosci. Methods 164, 177–190. https://doi.org/10.1016/j.jneumeth.2007.03.024.
Nunez, P.L., 1981. Electric Fields of the Brain: the Neurophysics of EEG. Oxford University Press.
O'Connell, R.G., Dockree, P.M., Kelly, S.P., 2012. A supramodal accumulation-to-bound signal that determines perceptual decisions in humans. Nat. Neurosci. 15, 1729–1735.
O'Connell, R.G., Shadlen, M.N., Wong-Lin, K., Kelly, S.P., 2018. Bridging neural and computational viewpoints on perceptual decision-making. Trends Neurosci. https://doi.org/10.1016/j.tins.2018.06.005.
Pfurtscheller, G., 1981. Central beta rhythm during sensorimotor activities in man. Electroencephalogr. Clin. Neurophysiol. 51, 253–264.
Philiastides, M., Heekeren, H.R., Sajda, P., 2014. Human scalp potentials reflect a mixture of decision-related signals during perceptual choices. J. Neurosci. 34 (50), 16877–16889. https://doi.org/10.1523/JNEUROSCI.3012-14.2014.
Preuschhof, C., Schubert, T., Villringer, A., Heekeren, H.R., 2010. Prior information biases stimulus representations during vibrotactile decision making. J. Cogn. Neurosci. 22, 875–887.
Ratcliff, R., Cherian, A., Segraves, M., 2003. A comparison of macaque behavior and superior colliculus neuronal activity to predictions from models of simple two-choice decisions. J. Neurophysiol. 90, 1392–1407.
Romo, R., Brody, C.D., Hernández, A., Lemus, L., 1999. Neuronal correlates of parametric working memory in the prefrontal cortex. Nature 399 (6735), 470–473.
Romo, R., Hernández, A., Zainos, A., 2004. Neuronal correlates of a perceptual decision in ventral premotor cortex. Neuron 41, 165–173.
Sanchez, G., 2014. PhD thesis. Real-time Electrophysiology in Cognitive Neuroscience: towards Adaptive Paradigms to Study Perceptual Learning and Decision Making in Humans, vol. 1. Université Claude Bernard Lyon, France.
Shadlen, M.N., Kiani, R., 2013. Decision making as a window on cognition. Neuron 80, 791–806.
Shadlen, M.N., Newsome, W.T., 2001. Neural basis of a perceptual decision in the parietal cortex (area LIP) of the rhesus monkey. J. Neurophysiol. 86, 1916–1936.
Shadlen, M.N., Britten, K.H., Newsome, W.T., Movshon, J.A., 1996. A computational analysis of the relationship between neuronal and behavioral responses to visual motion. J. Neurosci. 16, 1486–1510.
Shadlen, M.N., Kiani, R., Hanks, T.D., Churchland, A.K., 2008. Neurobiology of decision making: an intentional framework. In: Engel, C., Singer, W. (Eds.), Strüngmann Forum Reports. Better than Conscious? Decision Making, the Human Mind, and Implications for Institutions. MIT Press, Cambridge, MA, US, pp. 71–101.
Sherman, M.A., Lee, S., Law, R., Haegens, S., Thorn, C.A., Hämäläinen, M.S., et al., 2016. Neural mechanisms of transient neocortical beta rhythms: converging evidence from humans, computational modeling, monkeys, and mice. PNAS 113, E4885–E4894. https://doi.org/10.1073/pnas.1604135113.
Spitzer, B., Blankenburg, F., 2011. Stimulus-dependent EEG activity reflects internal updating of tactile working memory in humans. Proc. Natl. Acad. Sci. U.S.A. 108, 8444–8449.
Spitzer, B., Blankenburg, F., 2012. Supramodal parametric working memory processing in humans. J. Neurosci. 32, 3287–3295. https://doi.org/10.1523/JNEUROSCI.5280-11.2012.
Spitzer, B., Haegens, S., 2017. Beyond the status quo: a role for beta oscillations in endogenous content (re)activation. eNeuro 4. ENEURO.0170-17.2017.
Spitzer, B., Wacker, E., Blankenburg, F., 2010. Oscillatory correlates of vibrotactile frequency processing in human working memory. J. Neurosci. 30, 4496–4502.
Spitzer, B., Gloel, M., Schmidt, T.T., Blankenburg, F., 2014. Working memory coding of analog stimulus properties in the human prefrontal cortex. Cerebr. Cortex 24, 2229–2236.
Stokes, M.G., 2015. 'Activity-silent' working memory in prefrontal cortex: a dynamic coding framework. Trends Cognit. Sci. 19, 394–405. https://doi.org/10.1016/j.tics.2015.05.004.
Twomey, D.M., Murphy, P.R., Kelly, S.P., O'Connell, R.G., 2015. The classic P300 encodes a build-to-threshold decision variable. Eur. J. Neurosci. 42, 1636–1643.
Urai, A.E., Braun, A., Donner, T.H., 2017. Pupil-linked arousal is driven by decision uncertainty and alters serial choice bias. Nat. Commun. 8, 14637.
Van Ede, F., de Lange, F., Jensen, O., Maris, E., 2011. Orienting attention to an upcoming tactile event involves a spatially and temporally specific modulation of sensorimotor alpha- and beta-band oscillations. J. Neurosci. 31, 2016–2024.
van Kemenade, B.M., Seymour, K., Wacker, E., Spitzer, B., Blankenburg, F., Sterzer, P., 2014. Tactile and visual motion direction processing in hMT+/V5. Neuroimage 84, 420–427.
von Lautz, A.H., Herding, J., Ludwig, S., Nierhaus, T., Maess, B., Villringer, A., Blankenburg, F., 2017. Gamma and beta oscillations in human MEG encode the contents of vibrotactile working memory. Front. Hum. Neurosci. 11, 576. https://doi.org/10.3389/fnhum.2017.00576.
Wimmer, K., Ramon, M., Pasternak, T., Compte, A., 2016. Transitions between multiband oscillatory patterns characterize memory-guided perceptual decisions in prefrontal circuits. J. Neurosci. 13 (2), 489–505, 36.
Woodrow, H., 1935. The effect of practice upon time-order errors in the comparison of temporal intervals. Psychol. Rev. 42, 127–152.
Wu, Y., Uluç, I., Schmidt, T.T., Tertel, K., Kirilina, E., Blankenburg, F., 2018. Overlapping frontoparietal networks for tactile and visual parametric working memory representations. Neuroimage 166, 325–334.
Zaksas, D., Pasternak, T., 2006. Directional signals in the prefrontal cortex and in area MT during a working memory for visual motion task. J. Neurosci. 26 (45), 11726–11742.